An Eye in the Fog: Development of a Novel Navigational and Visual Guidance System for Aircraft Operations in Low Visibility Conditions

Siddharth Bharthulwar

A1 Background

Aircraft Operations in Low Visibility Conditions
https://flickr.com/photos/angelorangelo/16677860718
https://www.flickr.com/photos/gotfcharlie2332/16655879404/

Landing is the most difficult phase of flight with over 40% of fatal commercial aviation accidents. Poor weather conditions can make this procedure more difficult by obscuring crucial visual features a pilot must locate to land. A pilot's failure to identify these critical features can lead to fatal accidents. Nearly 450 people are killed in aviation accidents due to low visibility conditions every year (Mazon et al, 2018).

A2 Existing Solutions

Instrument Landing System (ILS), the current instrument-based navigation system, guides an aircraft until it reaches its decision height, when a pilot must be able to identify key features such as terrain, tall structures, and pertinent glideslope information. ILS systems use a series of localizers and radio transmitters to communicate with the aircraft to adjust heading and pitch.

A typical ILS localizer antenna installed at an airport
https://upload.wikimedia.org/wikipedia/commons/7/77/Tenerife_-_Localizer..JPG

ILS presents numerous disadvantages as well. ILS radio beams are easily disrupted by momentary obstructions to the transmitter and localizer, such as other traffic, leading to accidents. Due to this, ILS operations in low visibility warrant greater separation between aircraft, significantly increasing congestion at major airfields. Capable ILS systems are sparse due to their high cost (upwards of $5,000,00). The FAA estimates that only 2.5% of airports worldwide feature functional ILS systems, with even fewer zero visibility systems.

Runway excursion of Singapore Airlines Flight 327 following ILS transmission obstructions
https://code7700.com/images/singapore_airlines_327_aircraft_position.jpg

An infrared camera installed on an aircraft for navigation
https://m.aviationweek.com/sites/default/files/styles/crop_freeform/public/uploads/2016/10/bombardier-cvs-prop-2.png

Systems have been developed that use infrared sensors to map terrain obstacles in a pilot's FOV. However, these devices are proprietary and expensive. These vision systems cost upwards of $500,000. and provide an obscured/limited field of view of the current spatial environment and relevant data.

A3 Proposed Solution

A more accessible, robust, and feasible solution consists of a remote sensing based approach. Preexisting worldwide spatial databases and an aircraft's flight sensors can be leveraged. Novel algorithms can map these data and localize potential obstructions. An aircraft's ambient and inertial sensors record pertinent flight data that can be interpreted with deep learning. Based on the spatial mapping and sensor information data, the system can intelligently predict what a pilot sees outside of the cockpit window, even in fog. Flight hazards can be assessed through neural networks to prevent potential accidents while they are still recoverable. All these data can be presented in the pilot's direct field of view with a heads up display and 3D imagery. By projecting the parsed flight and terrain data onto an optical device, pilots can view both synthetic and real world data for greater spatial awareness.

Synthetically Rendered Surroundings and Flightpath

HUD overlaying flight data in pilot's FOV during final approach.
https://jetheal.files.wordpress.com/2013/03/huo-sample.jpg

A4 Engineering Goals

1. Accurately and Efficiently Map an Environment
Develop novel spatial mapping algorithms to preemptively identify, localize, and efficiently store pertinent spatial features and obstacles in a pilot's immediate surroundings.

2. Live Prediction of Future Trajectory and Flight Anomalies
Develop extended Kalman filters and neural network autoencoders to predict future trajectory and assess operational risks from aircraft sensor data.

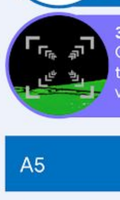

3. Display Pertinent Live Flight Data and Spatial Data in 3D
Combine navigational backend and reconstructed environment to predict and synthetically display an aircraft's surroundings as viewed through the pilot's current field of view.

A5 Solution Overview

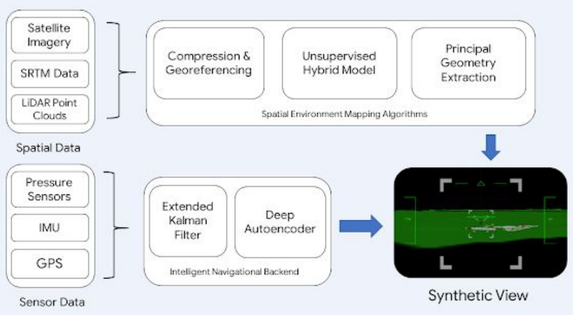

An aircraft's surroundings are preemptively mapped and exported to the graphical system. An aircraft's sensor measurements are iteratively updated and parsed by the intelligent navigational backend before being processed by the graphical system.

A6 Remote Sensing Datasets

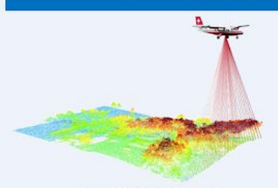

Aerial LiDAR Collection Technique
https://www.aanboom.net/wp-content/uploads/2014/10/lidar_operating_principles.jpg

LiDAR:
Surface LiDAR data were aerially recorded by the AHN, which spanned the entire Netherlands with vertical and lateral accuracies of ±15 cm & ± 10 cm. The datasets used in this investigation totaled ~ 657 gb with a point density of ~ 15 million points per square kilometer (Sande et al, 2010).

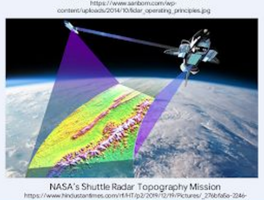

NASA's Shuttle Radar Topography Mission
https://www.hindustantimes.com/rf/image_size_960x540_wm/HT/p2/2019/10/19/Pictures/_37fd7d6e-f2e6-11e9-b7fb-55e416cd8533.jpg

SRTM:
Surface topography data were acquired from NASA's SRTM dataset. NASA used interferometry, a technique where two radar signals are emitted at different angles to the Earth's surface from a satellite/space shuttle. On average, the SRTM datasets have a RMSE of 4.73 meters (Van Zyl, 2017).

A7 Flight Model and Datasets

Aircraft have many sensors that continually record data, ranging from pressure sensors to inertial and inclination sensors. To parse these measurements and assess operational risks in live time, a comprehensive dataset was required. Aircraft flight data recorder (FDR) data were procured from the FAA, NTSB, and MIT's International Center for Air Transport. **The data were recorded on a wide range of aircraft, weather conditions, and trajectories to ensure a comprehensive model was built.**

A8 Georeferencing & Optimization

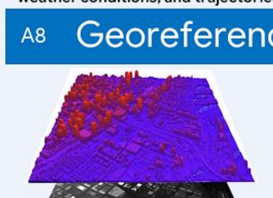

Fig. 1. Compression Process for LiDAR Data

LiDAR point clouds are dense with nearly 15,000,000 points per square km. To reduce data complexity and increase performance in the system, the 3D point clouds were flattened into a single plane. Anomalous LiDAR measurements from substances with irregular reflectivity or aerosols in the atmosphere are filtered through Gaussian smoothing. The single planes can be stored as 2D arrays, allowing for computer-vision-based approaches for mapping.

Fig. 2. Satellite Imagery of Airport

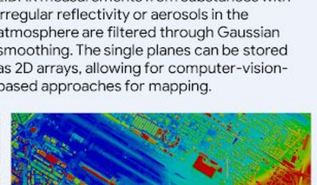

Fig. 3. Smoothened Elevation Data of Airport

All elevation data are automatically georeferenced with satellite imagery from the Landsat and Sentinel datasets through feature matching. Affine transformations are made on the LiDAR point clouds to match the dimensions of the real world. After georeferencing, all terrain data are synchronized with the movement of the aircraft even without a continuous GPS signal.

Spatial Environment Mapping

B1 Unsupervised Hybrid Model

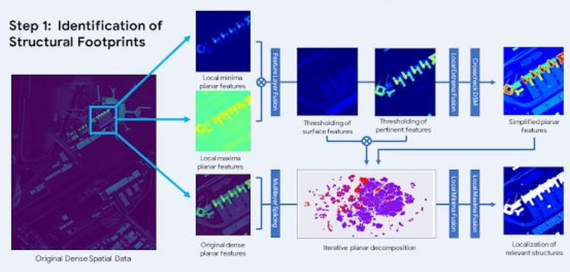

Convolution-based iterative detection approach. This step leverages the original dense LiDAR spatial data and local extrema to identify possible locations of terrain features and ground obstacles that may pose a threat to flight operations.

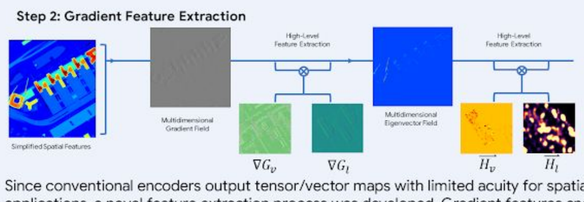

Since conventional encoders output tensor/vector maps with limited acuity for spatial applications, a novel feature extraction process was developed. Gradient features and eigenvector fields were the primary features extracted for lower level analysis.

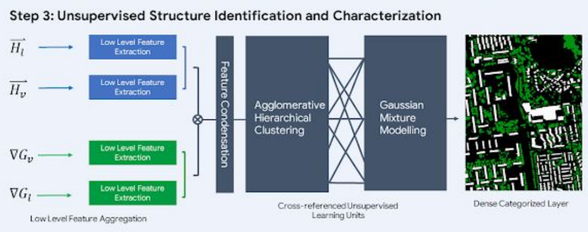

Schematic diagram of the unsupervised segmentation and localization process. Two unsupervised machine learning algorithms (AHC and GMM) cross-reference clustered feature data to identify pertinent structures in a pilot's predicted surroundings.

B2 Multimodal Unsupervised Learning

The unsupervised-network-based approach was opted for due to the wide Gaussian distribution of feature data in latent space and a lack of training data, which made conventional supervised CNN architectures unviable. By using unsupervised learning, the model is viable for any region of the world without additional training.

Fig 6. Agglomerative and Gaussian Clustering Dendrograms and Latent Space

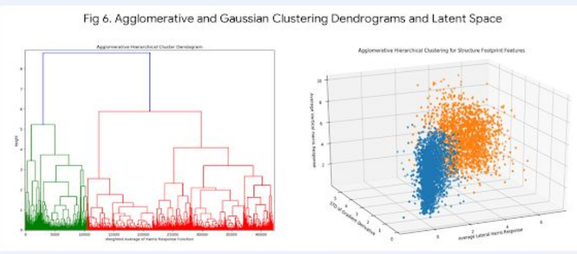

The Gaussian mixture models are parameterized by mixture component weights, the component means, and component covariances. For a multivariate Gaussian mixture model with K components, the k^{th}component has a mean of $\overrightarrow{\mu_k}$ and covariance matrix Σ_k. Without prior learned weights, the multi-dimensional Gaussian model is given as:

$$p(\vec{x}) = \sum_{i=1}^{K} \phi_i N(x \mid \mu_i, \Sigma_i), N(x \mid \mu_i, \Sigma_i) = \frac{1}{\sqrt{(2\pi)^K |\Sigma_i|}} \exp\left(-\frac{1}{2}(\vec{x} - \overrightarrow{\mu_i})^T \Sigma_i^{-1} (\vec{x} - \overrightarrow{\mu_i})\right), \sum_{i=1}^{K} \phi_i = 1$$

The agglomerative hierarchical clustering algorithms do not account for gaussian distribution, and are thus independently defined. After initial cluster centroid localization, both algorithms cross reference and pool cluster probabilities.

B3 Principal Geometry Extraction

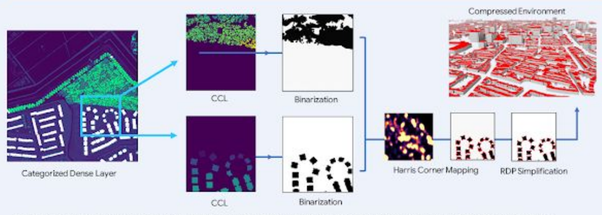

The principal geometry and topography of each structure is extracted through a computationally efficient pipeline consisting of iterated morphological operations. Sensor anomalies from aerosols or irregular reflectivity are filtered from the elevation profiles of each structure to reduce structural deformities in the final reconstruction.

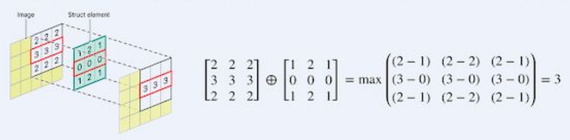

$$\begin{bmatrix} 2 & 2 & 2 \\ 3 & 3 & 3 \\ 2 & 2 & 2 \end{bmatrix} \oplus \begin{bmatrix} 1 & 2 & 1 \\ 0 & 0 & 0 \\ 1 & 2 & 1 \end{bmatrix} = \max \begin{pmatrix} (2-1) & (2-2) & (2-1) \\ (3-0) & (3-0) & (3-0) \\ (2-1) & (2-2) & (2-1) \end{pmatrix} = 3$$

Erosion and dilation, the specific morphological operations used to simplify planar geometry, work by convolving a structuring element over the digital surface model of a region (shown above). The structuring element is nonhomogeneous to compress surface geometry while maintaining relatively high spatial accuracy.

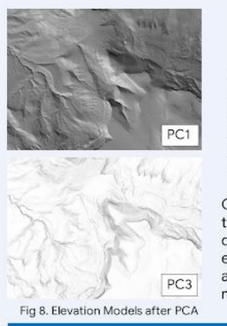

Fig 8. Elevation Models after PCA

Fig 7. Process for Principal Component Analysis

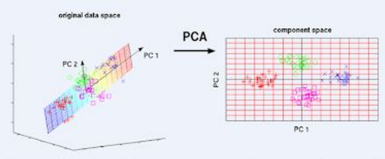

Ground terrain features are extracted and linearized through Principal Component Analysis. By reducing the dimensionality of lower-level spatial features, bare earth spatial data are compressed by nearly 67%, allowing for faster spatial analysis, storage, risk management, and display.

Intelligent Navigation Backend

B4 Extended Kalman Filter

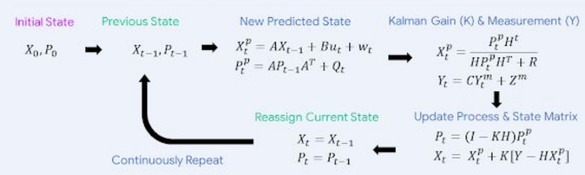

Fig N. Iterative Process of Extended Kalman Filter for State Estimation and Prediction

An extended Kalman filter is implemented to continuously predict an aircraft's current and future position and trajectory within a small margin of error. By iteratively adjusting Bayesian state biases for aircraft position, trajectory, and inclination, a continuous curve is generated for all pertinent flight data.

Fig 9. Filtered Sensor Time Series Measurements with Kalman Filter

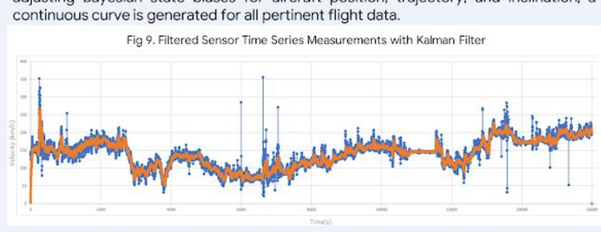

To reduce integration drift errors and sensor anomalies over time, the Kalman filter also removes anomalistic measurements in live time. This allows for a smoother and more accurate trajectory estimation from the velocity and inertial time series.

B5 Predictive Collision Avoidance

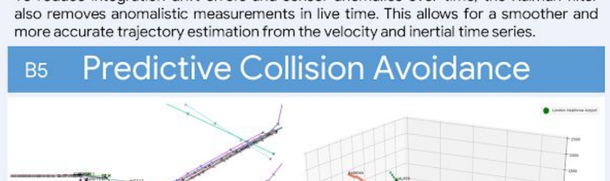

Fig. 10. 2D View of Intersecting Predicted and True Flightpaths

Fig. 11. 3D View of Predicted Flightpaths of Nearby Air Traffic

From ADS-B traffic data and a REST API, trajectories of other aircraft are aggregated. With the extended Kalman filter, the positions of other air traffic can be estimated for collision avoidance. Predictive intersection analysis measures collision risk between the aircraft and other air traffic within a standard gaussian position uncertainty.

C1 Deep Anomaly Autoencoder

Fig 12. Contextual Awareness in Kernel Density Estimated Time-Series Data

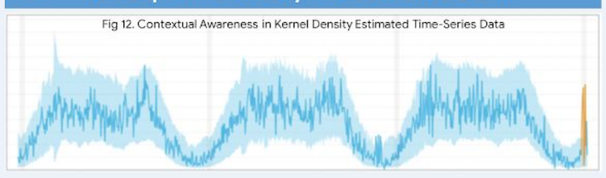

A kernel density estimation is calculated for all variables measured in real time. Representing each time series as a univariate distributed function f, with kernel K and bandwidth smoothing parameter h, the kernel density estimator is given as:

$$\hat{f}_h(x) = \frac{1}{n}\sum_{i=1}^{n} K_h(x - x_i) = \frac{1}{nh}\sum_{i=1}^{n} K\left(\frac{x - x_i}{h}\right)$$

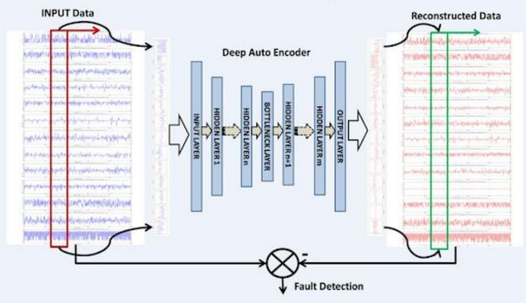

To predict and identify operational risks in real time, a self-supervised autoencoder is trained on time series data from aircraft. An autoencoder is a machine learning model that trains on its reconstructed output to build a comprehensive and distributed flight model for anomaly identification and prediction.

Fig 13. Real and Generative Aircraft Approaches from Variational Autoencoder

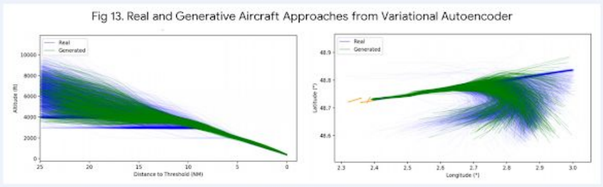

Pictured above, reconstructed flightpaths generated by the variational autoencoder with a noise vector mirror real flightpaths, indicating that the autoencoder was able to accurately train itself on realistic measurements.

C2 Synthetic Imagery

The previously parsed spatial and navigational data from the aircraft are used to predict the visual features of a pilot's surroundings in live time. An OpenGL environment was developed to display pertinent data in a pilot's field of view.

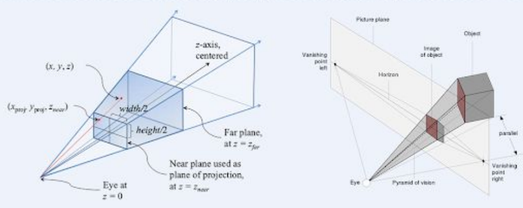

Fig 14. Projection Matrix-Based Field of View of 3D Graphical System

The guidance system has a virtually unlimited field of view since all visual aspects are computationally generated. The viewing frustum of the 3D scene was chosen to match that of the pilot while landing to accurately replicate the pilot's FOV. The eye of the system is integrated with the intelligent navigational backend to adjust according to aircraft movements with limited latency. Most flight data were presented in bright green light since the human eye is the most sensitive to those wavelengths of light.

Performance and build data were collected throughout the development process to optimize rendering and reduce latency between aircraft movements and synthetically replicated movements on the screen. The guidance system ran at an average of 75 fps with dedicated graphics and 47 fps with integrated graphics, indicating that the system is integrable with existing aircraft processors.

Results

C3 Spatial Environment Mapping

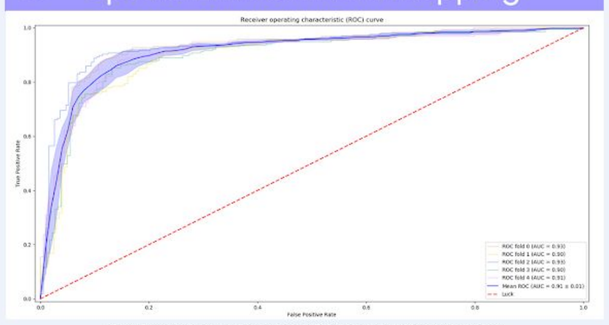

Fig. 15. Receiver Operating Characteristic (ROC) Curve for 5 Folds of Validation Data

The Receiver Operating Characteristic (ROC) curve was calculated for sets of original and manually annotated LiDAR data. These datasets were partitioned randomly with a k-fold process. **The system received a ROC AUC score of 0.91 ± 0.01, indicating a versatile model. The F1 classification accuracy was 98.0%.**

Fig. 16. Semantically segmented terrain structures in DSM from final localization and segmentation system

The semantically classified structure footprints were tested extensively with over 5,000,000 m² of manually annotated ground truth data. **The system segmented structures with a spatial Intersection over Union (IoU) accuracy of 97.3%.** Most topographical abnormalities and errors were generated by structures with complex geometries, indicating future research should work on building more robust segmentation algorithms for those cases.

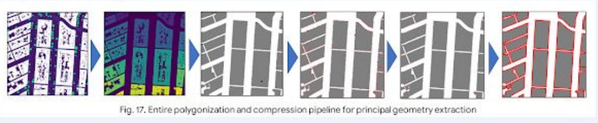

Fig. 17. Entire polygonization and compression pipeline for principal geometry extraction

On average, the spatial compression algorithms maintained an average of 98.7% accuracy while reducing vertex index sizes by an average of 65.6%. Stored structural bodies had an average of 7.2 vertices per structure. **After compression, the novel data structure and spatial mapping algorithms yielded data that were 29,346 times smaller than the original LiDAR and interferometry data.**

C4 Intelligent Navigation Backend

Fig 18. Continuous Path Generated with Kalman Filter

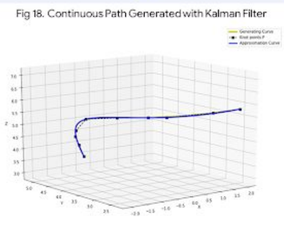

Fig 19. Simulated vs Measured Sensor Time Series

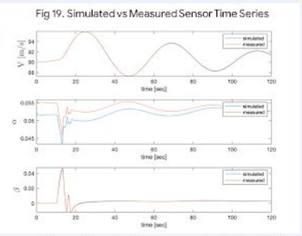

The extended Kalman filter was able to accurately estimate the current state of the aircraft as well as predict the future state of the aircraft during approach and landing. Across all variables, the filter estimated/predicted future states with an average RMSE of 3.72 ± 0.58 (in meters), **with an accuracy of 98.56% cumulatively.**

Fig 20. Individual Flight Measurements Compared to Gaussian Reconstruction from Autoencoder

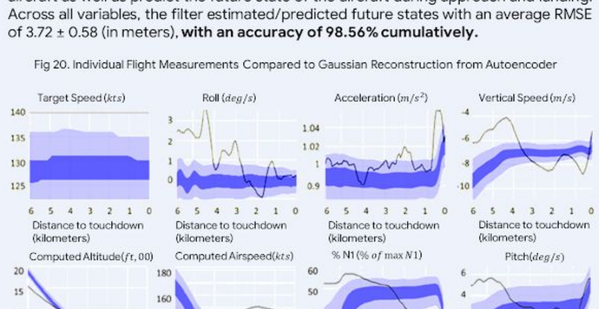

Theoretical testing on the extended Kalman filter and deep anomaly autoencoder reflect promising results. Based on the training data for the autoencoder, the intelligent system could predict operational anomalies 13.4 seconds (on average) before indications from existing hazard avoidance systems.

D1 Real World Validation & Results

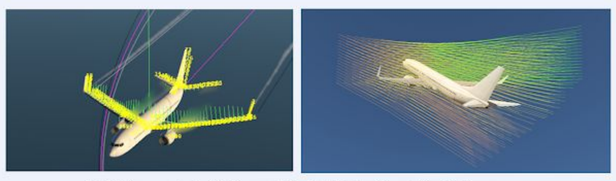

Fig 21. Screenshots of Advanced Flight Model of Simulation Software

Simulated testing occurred on professional-grade software with a realistic flight model, and found that the system was capable of both reconstructing an aircraft's predicted flightpath and predicting operational anomalies prior to occurrence. Testing on real world flight data indicated analogous results for estimation and prediction accuracy.

Fig 22. Extended Kalman Filter Prediction Accuracy (Simulated Flights)

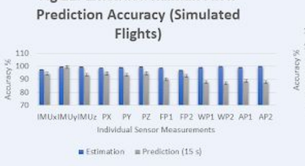

Fig 23. Extended Kalman Filter State Estimation and Prediction

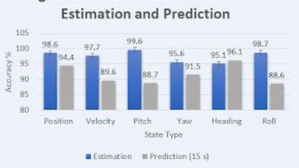

D2 Synthetic Rendering Results

D3 Computational Complexity

Preemptive Environment Mapping Algorithms

Algorithm	Complexity	Input Size
IDW Interpolation	$O(n^2)$	~ 1,000,000,000 per 50 km²
Adaptive Thresholding	$O(n^2)$	~ 125,000,000 per 50 km²
Connected Components	$O(n^2)$	~ 5000 per 50 km²
Gradient Features	$O(n^2 \log(n))$	~ 120,000 per 50 km²
Hierarchical Clustering	$O(n^3)$	~ 5000 per 50 km²
Gaussian Mixture Models	$O(2kn^3), k \in R^2$	~ 5000 per 50 km²
Erosion and Dilation	$O(nln(W)), W \in R^2$	~ 3000 per 50 km²
Harris Corner Detector	$O(n^2 log(n))$	~ 3000 per 50 km²
Ramer-Douglas-Peuker	$O(nlog(n))$	~1200 per 50 km²
Gaussian Filtering	$O(n^2)$	~1,000,000 per 350 km²
Polygon Triangulation	$O(nlog(n))$	~ 1500 per 50 km²

Live Time Guidance System & Navigational Backend

Algorithm	Complexity	Input Size
Kalman Filter Estimations	$O(nlog(n))$	~ 14 per second
Numerical Integration	$O(n)$	~ 300 per second
Trajectory Prediction	$O(n)$	~ 30 per second
Anomaly Autoencoder	$O(nlog(n))$	~ 14 per second
3D Guidance System	$O(1)$	N/A

D4 Hardware Implementation

The developed system is designed to run on current aircraft optical and flight management hardware. Heads up displays (HUDs) such as the one pictured (left) can display pertinent information from flight management computers in a pilot's immediate field of view. With an overhead projector and a properly collimated transparent optical combiner, pertinent real world metrics can be visualized at infinite focal length.

D5 Discussion

The developed guidance system successfully satisfied all design criteria. The spatial mapping algorithms were able to accurately and efficiently extract the geometry of relevant structures in dense LiDAR point clouds. Due to the effectiveness of the optimizations made during the data preprocessing phase, all aspects of this project ran in a computationally viable runtime. The performance data of the spatial mapping algorithms indicate that the system is scalable for worldwide usage.

The intelligent navigational backend was able to accurately estimate and predict current and future aircraft state and operational anomalies in real time. With transfer learning, the autoencoder model for flight data can be used on any twin-engine aircraft. The autoencoder and extended Kalman filter were successfully able to predict operational risks while they were recoverable and intelligently gave pilots the directions required to rectify the hazards.

The 3D synthetic imagery phase was successful, as all pertinent flight and obstruction data were displayed in accordance to their locations and values in real life. Minimal latency and high performance were observed in the graphical phase, indicating that the system can be implemented with existing aircraft hardware. The system was able to predict what the pilot would see outside of the cockpit regardless of visual conditions.

D6 Impact and Viability

The finished system is promising, as it has numerous advantages over current aircraft navigation systems. Estimated costs for the components of a heads up display (HUD) indicate that a physical display system could be produced for as little as $1200, making it significantly cheaper than current navigation systems while maintaining high accuracy and precision.

The remote sensing technology used in this project is increasingly viable for future use, as market predictions suggest dramatic increases in government investment. Most urban regions already have preexisting LiDAR and SRTM data. As the frequency of severe air pollution increases worldwide, the likelihood of airport runways being obscured in low visibility increases dramatically. Hence, proposed project will be increasingly necessary in the future as air pollution surrounding airports increases.

D7 Future Research

The most immediate direction of future work is to improve the sensitivity of the system to subtle aircraft movements, as the navigational backend and 3D imagery were unable to predict and display movements from light turbulence and headwinds, which may affect overall performance. Integration and testing on real aircraft hardware would provide advanced insights into the operational viability of the developed system.

Additionally, the self-supervised autoencoder was only tested on two aircraft from the same manufacturer with similar physical and mechanical characteristics. With a more comprehensive dataset, the versatility of the model could be tested with transfer learning on jet aircraft from other manufacturers with vastly different flight models and mechanical characteristics. With a flight data recorder dataset including smaller propeller aircraft and helicopters, the system can be trained to identify operational hazards on those types of aircraft as well.

D8 Referenced Work

Mazon, J. & Rojas, J. & Lozano, M. & Pino, D. & Prats, X. Influence of Meteorological Phenomena on Worldwide Aircraft Accidents 1967-2010. *Meteorological Applications*. 25: 236-245. (2018).
Sande, Corné & Soudarissanane, Sylvie & Khoshelham, Kourosh. (2010). Assessment of Relative Accuracy of AHN-2 Laser Scanning Data Using Planar Features. Sensors (Basel, Switzerland). 10. 8198-214. 10.3390/s100908198.
Van Zyl, Jakob. (2017). EE/GeS 157: *Interferometric Synthetic Aperture Radar 3*- I Notes, California Institute of Technology, Pasadena, California.
Fornberg B. (1988) Generation of Finite Difference Formulas on Arbitrarily Spaced Grids, Mathematics of Computation 51, no. 184: 699-706.
Wu, Kesheng & Otoo, Ekow & Suzuki, Kenji. (2009). Optimizing two-pass connected-component labeling algorithms. Pattern Analysis & Applications. 12. 117-135. 10.1007/s10044-008-0109-y.
Tibshirani, Ryan. (2013). Stats 10-705: *Clustering 2: Hierarchical Clustering Lecture Notes*, Carnegie Mellon University, Pittsburgh, Pennsylvania.
Zambrano, Jesús. (2017). Gaussian Mixture Model - method and application. 10.13140/RG.2.2.32667.77602.
Long, Nguyen Xuan. (2012). Clustering Problems, Mixture Models, and Bayesian Nonparametrics. University of Michigan, Ann Arbor, Michigan.
Kuhn, M., & Johnson, K. (2016). *Applied predictive modeling*. New York: Springer.
(2019). *Morphological Image Processing Lecture Notes*: 2019-7, Stanford University, Stanford, California.
Hershberger, John & Snoeyink, Jack. (1994). An O(nlogn) Implementation of the Douglas-Peuker Algorithm for Line Simplification. *Association for Computing Machinery*, New York, New York, 383-384.
Tasdizen, Tolga & Whitaker, Ross. (2003). Feature Preserving Variational Smoothing of Terrain Data. University of Utah, Salt Lake City, Utah.
Zhang, Jun & Liu, Wei & Zhu, Yanbo. (2011). Study of ADS-B data evaluation. Chinese Journal of Aeronautics - CHIN J AERONAUT. 24. 461-466. 10.1016/S1000-9361(11)60053-8.
Gong, Boyuan & Li, Wenbo & Shen, Zhiyuan. (2017). An ADS-B Trajectory Segmentation Correction Algorithm Based on Improved Kalman Filtering. 10.2991/amms-17.2017.12.
Zhang, Mengde & Li, Kailong & Hu, Baiqing & Meng, Chunjian. (2019). Comparison of Kalman Filters for Inertial Integrated Navigation. Naval University of Engineering, Wuhan, China.
Ge, Aiming & Song Xianjie & Wei, Minchen. (2009). Design for a Measurement System of Led Precision Approach Path Indicator Lights. *Light and Engineering* 17(4): 63-65.

All images, diagrams, charts, and graphs, unless specifically cited, were created by Siddharth Bharthulwar.